Solar-Terrestrial Physics. 2026, vol. 12, iss. 1, pp. 18–21. DOI: 10.12737/stp-121202603.

DOI: 10.12737/stp-121202603
EDN: DWIEAV

Received June 16, 2025
Accepted October 01, 2025

SPACE DEBRIS EFFECT ON SOLAR RADIATION PROPAGATION

S.S. Veniaminov
Central Research Institute of Aerospace Forces,
Ministry of Defense of the Russian Federation,
Moscow, Russia, sveniami@gmail.com

S.I. Kozlov
Central Research Institute of Aerospace Forces,
Ministry of Defense of the Russian Federation,
Moscow, Russia, s_kozlov@inbox.ru
Sadovsky Institute of Geosphere Dynamics RAS,
Moscow, Russia

M.Yu. Kuzmicheva
Sadovsky Institute of Geosphere Dynamics RAS,
Moscow, Russia, mukuzmgm@gmail.com

Abstract. The growing amount of space debris (SD) in near-Earth space already poses a threat to space activities, interferes with astronomical observations, and may lead to negative environmental consequences on Earth in the future. This paper estimates the current attenuation of solar radiation in the wavelength range from vacuum ultraviolet to infrared. We determine the rate of exponential increase in SD mass. Estimates of the future SD mass are also obtained at which the logarithm of solar radiation attenuation will increase to 10^{-6}–10^{-3}. We find the time required for the logarithm of solar radiation attenuation to increase to 10^{-6}.

Keywords: space debris, solar radiation, environmental safety.

INTRODUCTION

Currently, it is becoming increasingly obvious that the uncontrolled continuous growth of space debris (SD), especially small ones, in near-Earth space poses a real threat to human activity in space [Veniaminov, 2023; Adushkin et al., 2019]. First, the probability of collision of multipurpose operating spacecraft (SC), located in different orbits, with SD increases. Second, practicing astronomers note that in some cases SD already affects their observations in the optical spectral range. Third, Adushkin et al. [2019] observe that over time the contamination of near-Earth space can affect propagation of solar radiation, thereby leading to very negative environmental consequences on Earth.

The purpose of this paper is to estimate the critical mass of SD, which will begin to have a noticeable effect on solar radiation.

1. INITIAL DATA, MAN-MADE ASSUMPTIONS

To model parameters, we have used the data on particle fluxes on the spacecraft surface, as well as their size distribution. The data on particle fluxes was taken from [Adushkin et al., 2019; Manis et al., 2021].

We employed values of SD fluxes in different orbits: at altitudes 800–900, 400–450 (the orbit of the International Space Station, ISS), and 560–620 km (the orbit of the Hubble telescope). The papers deal with fluxes for SD of different sizes. Minimum sizes of fragments for which experimental data is available are 2000 μm (2 mm) at altitudes to 1000 km (according to observations by the Goldstone and HUSSAR radars) and 100 μm (0.1 mm) for measurements from the number of impacts on the spacecraft surface.

Figure 1 shows the number of known cataloged large ($\gtrsim$10 cm) space objects (SO) in 10 km zones at various altitudes in low orbits for different time epochs [Veniaminov, 2023].

Diverse objects in space generate SD, although not all of them relate to it. With the years, contamination increases [Adushkin et al., 2019; Derelict ..., 2023; Three ..., 2024].

Figure 2 illustrates SD flux F dependences on the particle diameter D at altitudes 560–620 km. Solid curves indicate distributions obtained by the ORDEM-3.1 (curve 1) and MASTER-8 (curve 2) models [Manis et al., 2021]; dashed curves are approximations of these distributions by power functions of the type

$$F\left(d < D\right) = AD^{-b}, \tag{1}$$

where A and b are constants; d is the smallest diameter. At the same time, for the two distributions considered we found

$$A_1=3504998.47,\ b_1=2.354611, \tag{2}$$

$$A_2=60420.74,\ b_2=1.610146. \tag{3}$$

The model distributions were matched with the measurement data only in the range of particle sizes 100–300 μm [Manis et al., 2021], in which (see Figure 2) both distributions are very close. When going to smaller sizes, we should take into account that the distribution function is not precisely known, so in the calculation we examine both distributions (2) and (3).

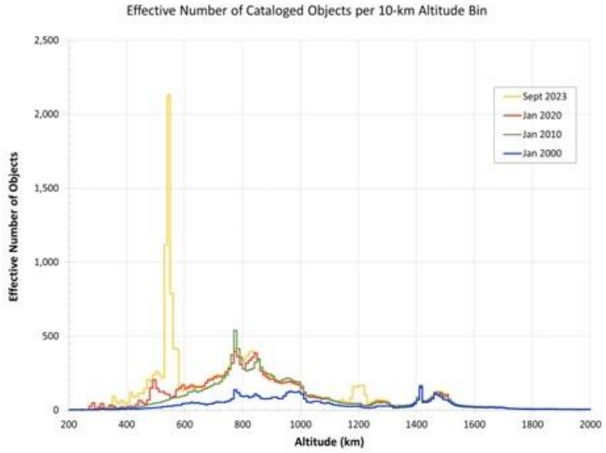

Figure 1. The number of SO in 10 km zones at various altitudes in low orbits

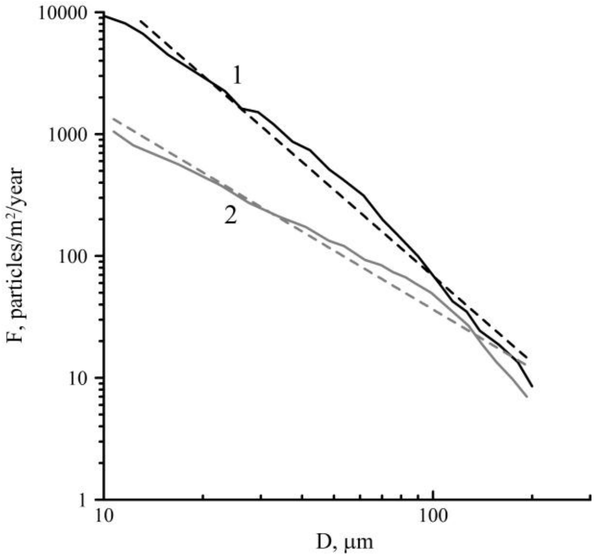

Figure 2. Model SD fluxes as a function of size

The spectral range of solar radiation analyzed in the paper is from 0.1 to 100 µm. This range includes the vacuum ultraviolet region containing the Lyα, Lyß lines responsible for the ionization of the lower and middle ionosphere, parts of visible radiation, as well as near and far infrared radiation, which plays an important role in Earth's thermal balance.

We explored only SD fragments in circular orbits. They were supposed to be evenly distributed along the trajectory of the spacecraft, the impacts on the surface of which determined the flow of matter, and particle concentrations were expected to be the same in an altitude range Δh~50 km near the spacecraft orbit.

It was also assumed that at different altitudes the size distributions of SD have the same power b, but different A coefficients. They are listed in Table 1 (for b from (2)). Figure 2 shows the A coefficients for 560 km (the orbit of the Hubble telescope). At 400 km (ISS orbit) and 800 km (sun-synchronous orbit), they were obtained from similar model dependences derived in [Manis et al., 2021]. For 1200 km, the altitude distribution of SO masses was used (see [Adushkin et al., 2019], Figure 4). The SD flux at 800 km was scaled by the ratio of masses to orbital lengths for 1200 and 800 km for the flux at 1200 km.

Table 1

Altitude dependence of A coefficients

Altitude, km	A coefficient
1200	$2.22\ 10^6$
800	$4.10\ 10^7$
560	$3.58\ 10^6$
400	$4.10\ 10^5$

To turn from the particle fluxes per year to their concentrations per unit volume, we calculated the path length that the SD particle detector travels during the year. To determine concentrations at altitudes below 400 km, we employed the altitude distribution of SO masses from [Adushkin et al., 2019] and the concentration at 400 km; for altitudes above 1200 km, the same mass distribution and concentration at 800 km.

SD concentrations in intermediate orbits were found through logarithmic interpolation. Consideration was given to the altitude range from 200 to 1800 km.

Although the shape of SD fragments in most cases is not spherical (see the shape distribution in [Greene, 2024; Cowardin et al., 2024]), the Mie approximation was employed to calculate the extinction cross section s_{ext} depending on the diameter D and the radiation wavelength λ [Timofeev, Vasil'ev, 2003]. The input parameters for the calculation program, in addition to D and λ, were the real and imaginary parts of the refractive index n of SD material. The SD fragments were thought to consist of aluminum [Bernhardt et al., 1993] since it is known that metals predominate in SD: Al, Fe, a little Cu and Ti [Cowardin et al., 2024]. The refractive index of aluminum used in the calculations was derived from measurements at λ=0.589 µm [Gurevich, 1983]. There is no data on other wavelengths, which is why the refractive index dispersion is ignored at this modeling stage.

The attenuation coefficient by Al particles $\alpha_{\text{Al}}(h, \lambda)$ was determined from the equation

$$\alpha_{\text{Al}}(h,\lambda)=\sum s_{\text{ext}}(D_k,\lambda)N(D_k). \tag{4}$$

Here, $N(D_k)$ is the concentration of SD with diameters D_k–D_{k+1} at an altitude h. The summation was over a range of SD sizes.

When calculating attenuation of solar radiation, a single scattering was taken into account due to the obvious rarefaction of SD. Solar radiation in the atmosphere was assumed to propagate vertically.

The differential equation of radiation transfer along a beam in the absence of radiation from the medium per se is written as follows:

$$dI(\lambda)/dh=-\alpha(\lambda)I(\lambda). \tag{5}$$

Where I is the radiation intensity, h is the coordinate along a beam, and α is the volume attenuation coefficient (wavelength indices are omitted). In the atmosphere for the addition of gas and aerosol characteristics, the following expression is valid

$$\alpha=\alpha_{\text{mol}}+\alpha_a, \tag{6}$$

where α_{mol} is the contribution to attenuation of gas components; α_a is the contribution of aerosols [Timofeev, Vasil'ev, 2003]. In our model,

$$\alpha=\alpha_{\text{atm}}+\alpha_{\text{Al}}, \qquad (7)$$

where α_{atm} and α_{Al} are the coefficients of attenuation by the atmosphere and SD fragments. In view of $\alpha(h)$, solution of (5) is written as

$$I(h)=I_0\exp\left(-\int_0^h \alpha(h')\,dh'\right). \qquad (8)$$

Here, I_0 is the initial intensity value (at h=0). $P=I(h)/I_0$ is the transmission function of the atmospheric layer h in thickness [Timofeev, Vasil'ev, 2003]. P can be represented as follows (7):

$$P=\exp\left(-\int_0^h \alpha(h')\,dh'\right)= \\ =\exp\left(-\int_0^h \alpha_{\text{atm}}(h')\,dh'\right)\exp\left(-\int_0^h \alpha_{\text{Al}}(h')\,dh'\right). \qquad (9)$$

We neglect atmospheric absorption (α_{atm}=0). In this case, the transmission function $P(\lambda)$ is defined by the equation

$$P(\lambda)=\exp\left(-\int_{h_1}^{h_2} \alpha_{\text{Al}}(h,\lambda)\,dh\right). \qquad (10)$$

2. SIMULATION RESULTS AND THEIR DISCUSSION

Figure 3 plots transmission functions versus wavelength (curves 1 and 2) for SD size distributions with powers b_1 and b_2 (2), (3).

The simulation results suggest that SD size distributions are essential for critical assessment of SD effect on solar radiation.

The radiation attenuation is maximum for distribution option (2) in the visible range and is ~$5\cdot10^{-8}$. The resulting attenuation of the solar radiation flux is negligible and is not a significant factor that would affect human activity at the present time. In order for the attenuation to reach, say, 10^{-6}, the number of fragments must grow 20 times. Accumulation of such a mass of small SD fragments can occur in about 50 years at the current rate of mass growth.

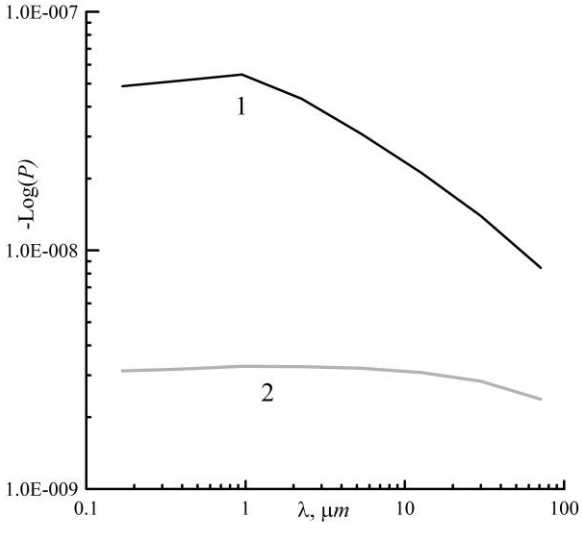

Figure 3. Transmission functions versus wavelength for two distributions (2), (3)

The rate of mass growth was estimated from the data collected by Adushkin et al. [2019]. The value 10^{-6} for the logarithm of radiation attenuation is chosen in such a way that the period during which the SD mass increases exponentially would be no more than a few decades. The mass growth with time was estimated for the rate of mass growth relevant to 2015 (as determined from the data presented in Figure 2 in [Adushkin et al., 2019]). Low-orbit spacecraft constellation has rapidly increased for 5–7 years. The rate of SD mass growth should be expected to rise.

We also calculated the current mass M of SD column for the two size distributions mentioned above. The results are presented in Table 2. Table 3 shows masses of SD column for increasing attenuation of solar radiation.

Table 2

Masses of SD column
for size distributions (2) and (3)

Mass M, kg/m^2:	$2.88\ 10^{-10}$	$8.16\ 10^{-11}$
Option:	1	2
Maximum attenuation of solar radiation –log(P)	$5.46\ 10^{-8}$	$3.27\ 10^{-9}$

Table 3

Masses of SD column
for size distributions (2) and (3)
with attenuation 1.0 $10^{-6}$and 1.0 10^{-3}

Maximum attenuation of solar radiation 1.0 10^{-6}	Mass, kg/m^2, Option 1: 5.28 10^{-9}	Mass, kg/m^2, Option 2: 2.50 10^{-8}
Maximum attenuation of solar radiation 1.0 10^{-3}	Mass, kg/m^2, Option 1: 5.28 10^{-6}	Mass, kg/m^2, Option 2: 2.50 10^{-5}

CONCLUSIONS

Our assessment of the critical SD mass with the aid of the described model shows that its exponential increase can pose a potential threat to the environment. According to estimates of the current rate of accumulation of particle mass, the logarithm of solar radiation attenuation due to SD up to 10^{-6} may increase in about 50 years. At present and in the near future, attenuation of solar radiation due to SD is not a significant factor that would affect human activity.

The work was carried out under Government Assignment of the Ministry of Science and Higher Education of the Russian Federation (Project No. 125012200624-5).

REFERENCES

Adushkin V.V., Aksenov O.Y., Veniaminov S.S., Kozlov S.I. On the assessment of the danger of small space debris for space activities and ecology. *Vozdushno-kosmicheskaya sfera*. [Aerospace Sphere] 2019, no. 3, pp. 72–81. DOI: 10.30981/2587-7992-2019-100-3-72-81. (In Russian).

Bernhard R., Barrett R.A., Zolensky M.E. Analytical electron microscopy of LDEF impactor residues. *"LDEF 69 Months in Space" 3-rd Postretrieval Symposium.* Williamsburg, VA (United States). 1993, pt. 1, pp. 401–427.

Cowardin H., Opiela J., Liou J.-C., King A., Melo DebriSat J. DebriSat: 10 Years and Growing. *ODQN.* 2024, vol. 28, iss. 4, pp. 5–8.

Derelict cosmos communications spacecraft breaks up in June 2023. *ODQN.* 2023, vol. 27, no. 4, pp. 1–2.

Greene R. Aerodynamic demise model for carbon fiber reinforced polymer. *ODQN.* 2024, vol. 28, no. 4, pp. 3–5.

Gurevich M.M. *Photometry.* L., Energoatomizdat Publ., 1983, 272 p. (In Russian).

Manis A., Matney M., Vavrin A., et al. Comparison of the NASA ORDEM 3.1 and ESA MASTER-8 models. *ODQN.* 2021, vol. 25, no. 3, pp. 2–4.

Three new on-orbit fragmentations. *ODQN.* 2024, vol. 28, no. 4, pp. 1–2.

Timofeev Y.M., Vasil'ev A.V. *Theoretical foundations of atmospheric optics.* Saint Petersburg, Nauka Publ., 2003, 474 p. (In Russian).

Veniaminov S.S. *Space debris. Man-made space pollution and its consequences*. Moscow: IKI RAN Publ., 2023, 204 p. DOI: 10.21046/spacedebris-2023. (In Russian).

Original Russian version: Veniaminov S.S., Kozlov S.I., Kuzmicheva M.Yu., published in Solnechno-zemnaya fizika. 2026, vol. 12, no. 1, pp. 21–24. DOI: 10.12737/szf-121202603.

How to cite this article

Veniaminov S.S., Kozlov S.I., Kuzmicheva M.Yu. Space debris effect on solar radiation propagation. *Sol.-Terr. Phys*. 2026, vol. 12, iss. 1, pp. 18–21. DOI: 10.12737/stp-121202603.